Supplementary Information for: Integrating DNA Strand Displacement Circuitry with DNA Tile Self-assembly

David Yu Zhang*; Rizal F. Hariadi*; Harry M. T. Choi, and Erik Winfree

(Dated: June 1, 2013)

Table of Contents:

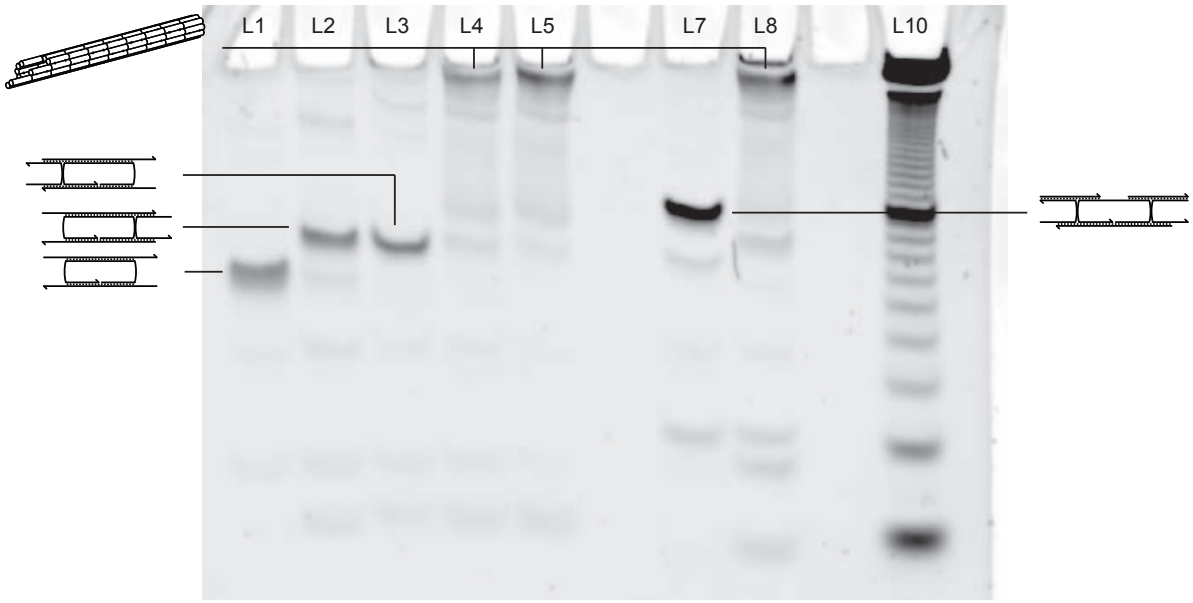

Supplementary Figure S1: Native polyacrylamide gel electrophoresis of DNA tile self-assembly. Here we verify the formation and consumption of the incomplete and protected tiles, and also to qualitatively verify the isothermal assembly of DNA nanotubes. The incomplete and protected tiles were previously gel purified. The existence of lower (faster migrating) bands in lanes 2 and 7 suggests that a fraction of these tiles are dissociating during the gel running process. Upon addition of the activator/deprotector, monomer tiles are completely consumed and migrated as higher molecular weight species. There is no control over the length distribution of the DNA nanotubes in the current system, and furthermore, some of the DNA nanotubes may have dissociated during the gel running process; consequently, a combination of these factor contribute to the distribution of high molecular weight species. The purpose of this gel, however, is to show the formation and subsequent assembly of the incomplete and protected tiles. Gel running conditions were 10% acrylamide, 25 °C (controlled by external temperature bath), 120 V for 100 minutes; the gel was cast in a Novex Mini-cell cassette (8 cm by 8 cm) purchased from Life Technologies. Species were 100 nM in reaction solution before being loaded onto the gel.

L1	The incomplete tile (method 1).
L2	The incomplete tile and the right activator, incubated at 25 °C for 1 hour.
L3	The incomplete tile and the left activator, incubated at 25 °C for 1 hour.
L4	The incomplete tile and both activators, incubated at 25 °C for 1 hour.
L5	The incomplete tile and both activators, thermally annealed.
L7	The protected tile (method 3).
L8	The protected tile and the deprotector, incubated at 25 °C for 1 hour.
L10	10 nt duplex ladder.

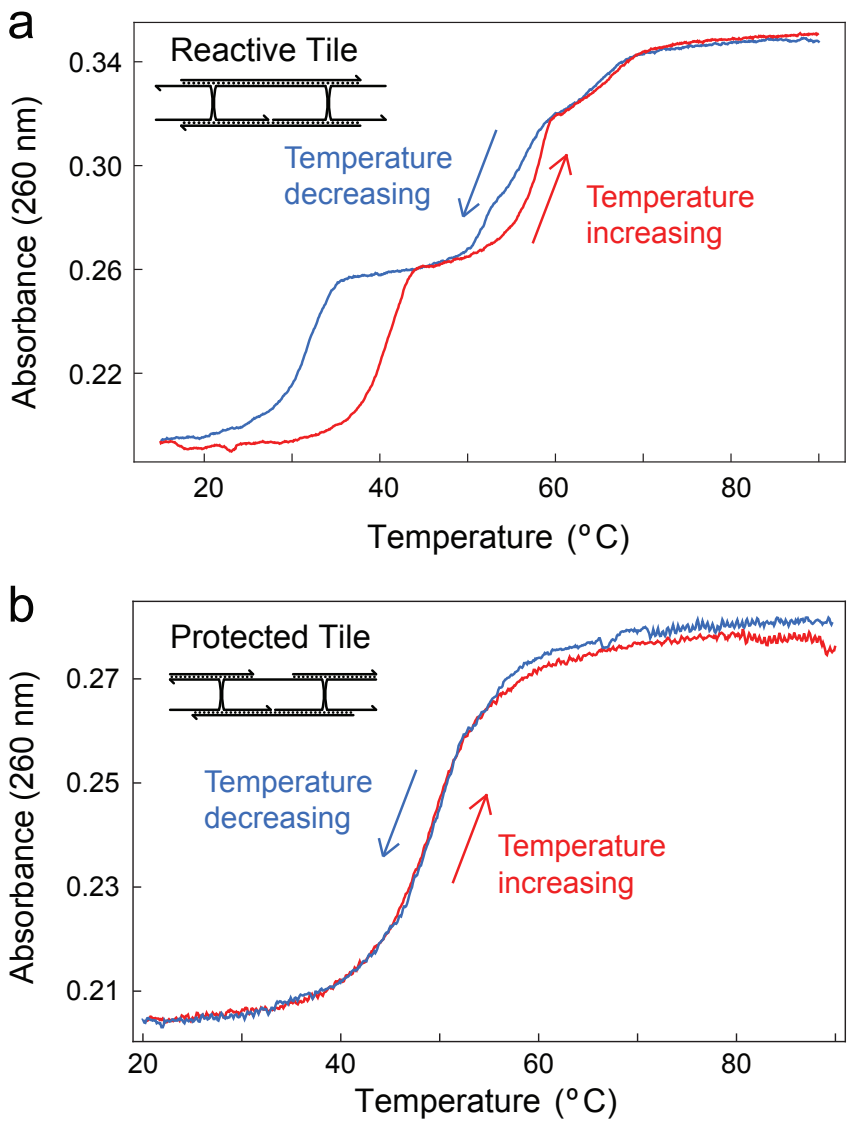

Supplementary Figure S2: UV absorbance annealing and melting curves of DNA tile self-assembly. Absorbance at 260 nm of the **(a)** reactive tiles and **(b)** protected tile (200 nM) at various temperatures. The sequences of strand for the reactive tile shown in panel (a) differ slightly from that used in the majority of our experiments, although the design of the tile is otherwise identical. Its sequences are shown in ref. 18 of the main paper, where the tile is called "SEs". The red trace shows the absorbance as the temperature was increasing, and the blue trace shows the absorbance as the temperature was decreasing. In panel (a), both the red and blue curves show a plateau near 0.26 absorbance; this likely corresponds to the reactive tile in the absence of DNA nanotube assembly. During the annealing (cooling) curve, the reactive tiles do not assemble until 34 °C, while in the melting (heating) curve, the DNA nanotubes do not dissociate until 42 °C. This hysteresis is likely due to the kinetic barrier of nucleation. In panel (b), there is no hysteresis and no plateau, implying that the protected tile does not undergo further aggregation or assembly.

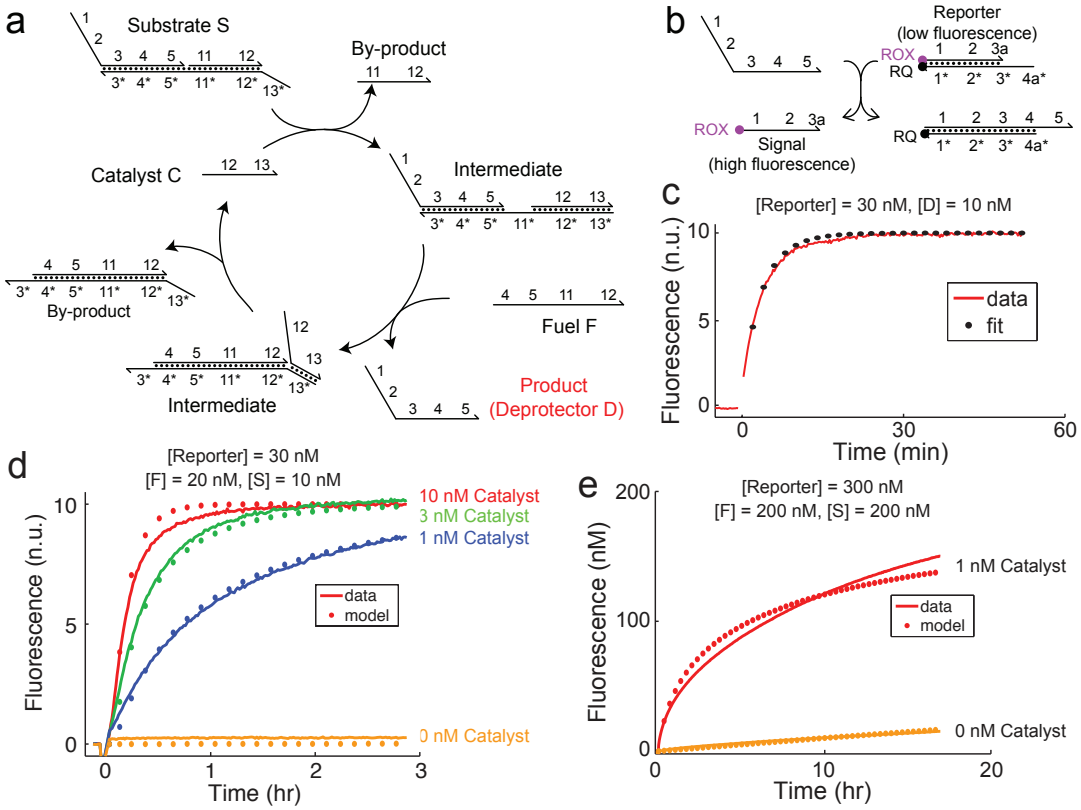

Supplementary Figure S3: Characterization of the upstream catalytic pathway. **(a)** The schematic of the catalytic pathway. Catalyst C binds to substrate S via the latter's 13* domain, and displaces the 11:12 by-product through a strand displacement reaction. The intermediate possesses a single-stranded 11* domain, which initiates reaction with the single-stranded 11 domain on fuel F. At the end of the catalytic cycle, the deprotector D is released as a product, and the catalyst is released to allow multiple turnover. **(b)** To assay the kinetics of the catalysis system, a fluorophore-labeled reporter complex that stoichiometrically reacts with the deprotector was used. The reporter itself yields low fluorescence, but upon reaction with the deprotector, the released released strand is unquenched and exhibits high fluorescence. ROX denotes the carboxy-X-rhodamine fluorophore, and RQ denotes the Iowa Black Red Quencher. The 3a and 4a* domains are each 5 nt long, and are respectively 5'-GAGAC-3' and 5'-TTGCT-3'. **(c)** Kinetics of reporter activation. The best fit rate constant for the reaction between the deprotector and the reporter complex is $1.9 \cdot 10^5$ M^{-1} s^{-1}, corresponding to a reporting delay of about 8 minutes for 30 nM reporter. Note that this rate constant is NOT used for the kinetic modeling of the integrated system shown in the main text Fig. 5, as no fluorescent reporter was present there. **(d)** Kinetics of catalysis. The initial production rate of the deprotector varies with the catalyst concentration. Sub-stoichiometric quantities of catalyst (relative to F and S) can nonetheless drive the reaction to completion, indicating multiple catalytic turnover. For comparison, the dotted lines show the model of equations (1-4) of the main text. **(e)** Long-term catalysis behavior. The red trace shows the production rate of deprotector D with 1 nM catalyst, while the orange trace shows the production rate of deprotector D in absence of catalyst (leak reaction). Over the course of 18 hours, 1 nM catalyst yields the release of over 110 nM of deprotector in excess of the leak reaction, corresponding to an average turnover of over 110. For comparison, the dotted lines show the model of equations (1-4) of the main text.

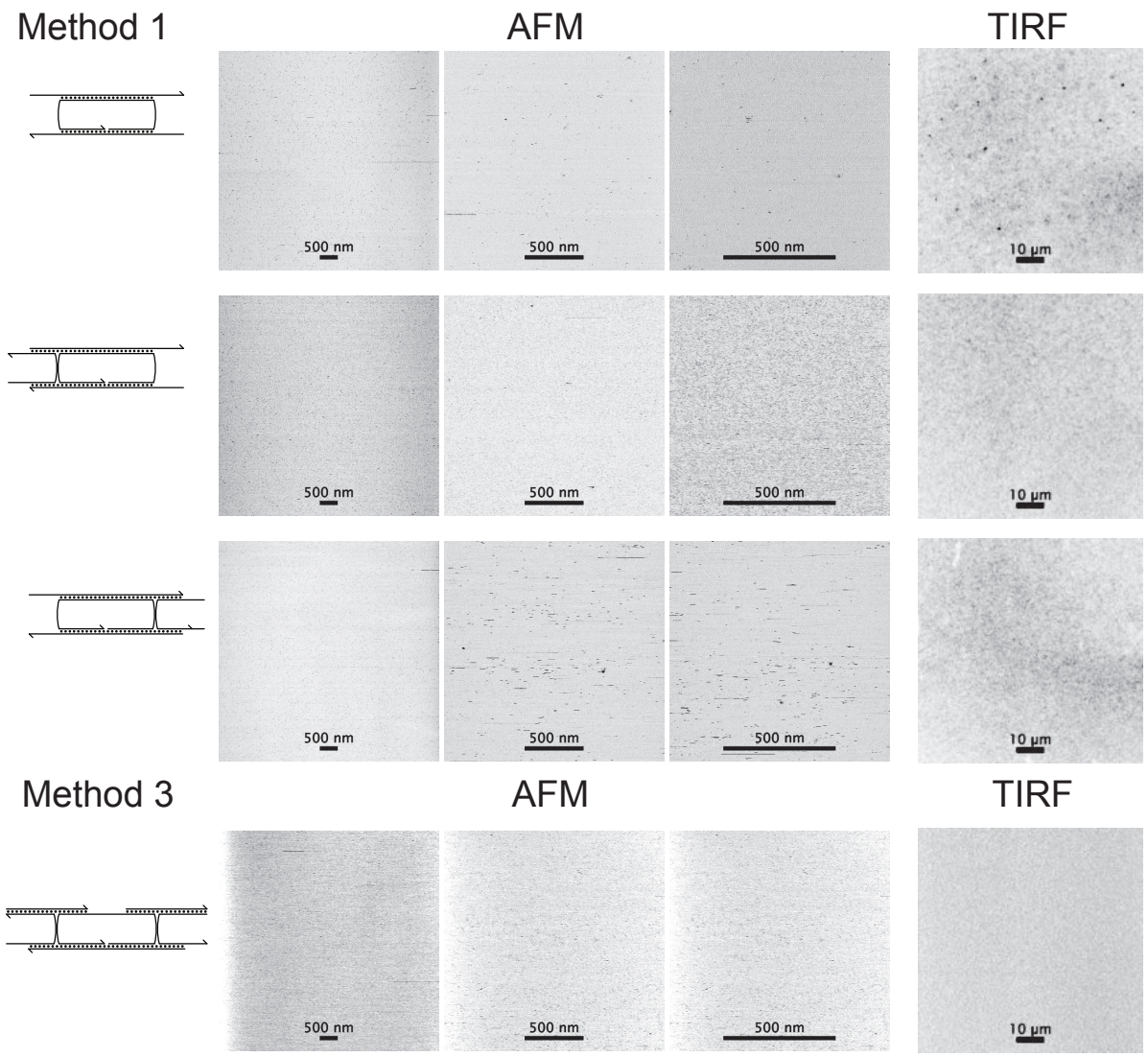

Supplementary Figure S4: Additional AFM and TIRF experiments (negative) on triggered DNA nanotube assembly. DNA nanotubes are not expected to form in these experiments. In method 1, the incomplete tile is not observed to form DNA nanotubes when either activator is absent. In method 3, the protected tile is not observed to form DNA nanotubes when the deprotector is absent. In all experiments, the concentrations of all species were 200 nM. In all experiments, the reactants were mixed and allowed to react at room temperature (25 °C) for 2 hours prior to imaging.

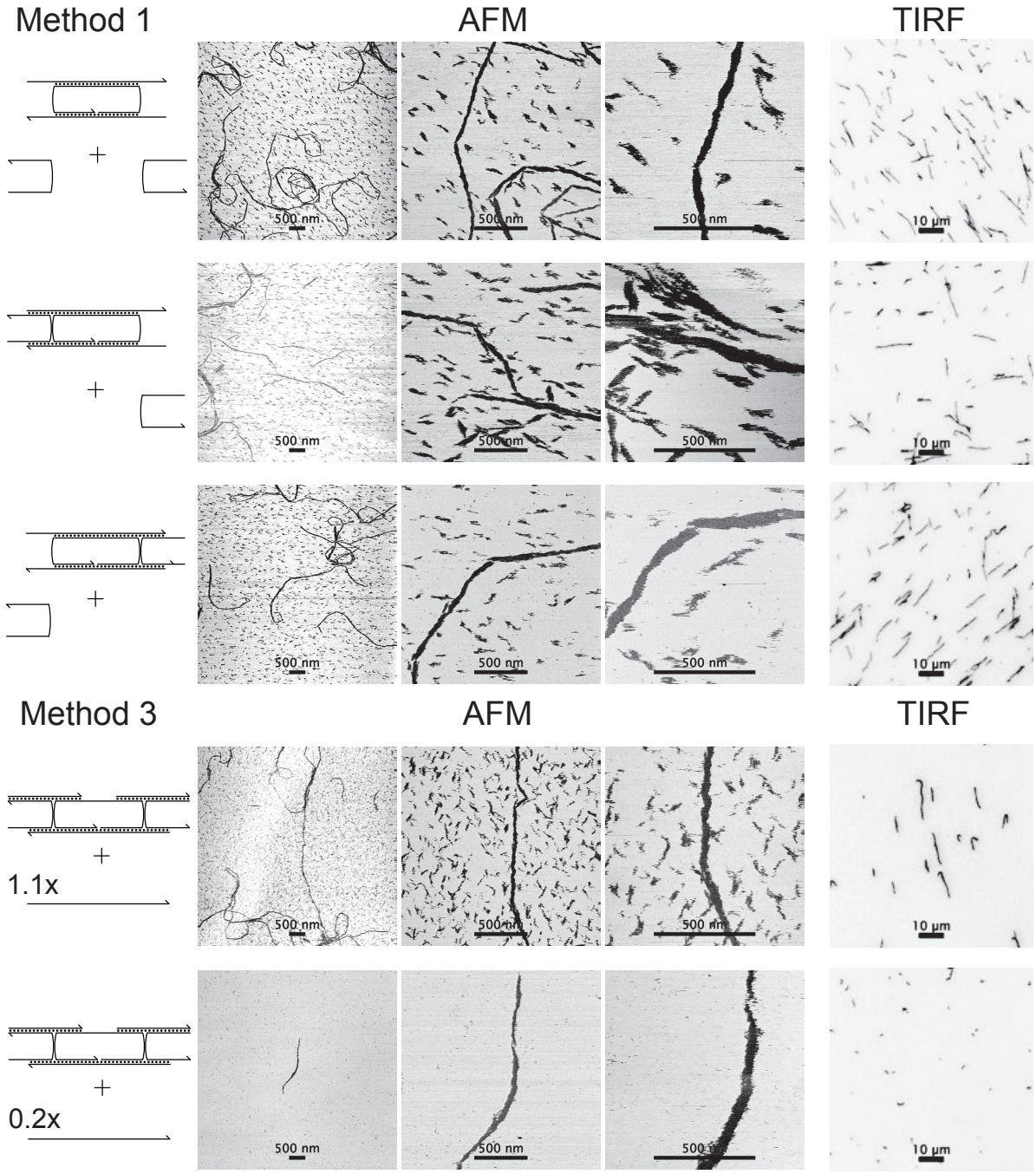

Supplementary Figure S5: Additional AFM and TIRF experiments (negative) on triggered DNA nanotube assembly. DNA nanotubes are expected to form in these experiments. In method 1, the reactive tile is isothermally reconstituted in one of three ways: reacting the incomplete tile with both activators, or pre-annealing the incomplete with one activator and subsequent isothermal reaction with the other activator. In all three case, DNA nanotubes were expected to form. In method 3, the reactive tile is isothermally reconstituted by reacting the protected tile with the deprotector. When a substoichiometric quantity of deproctector was added, then very few nanotubes are formed in the allotted time. The nonlinearity in the number of nanotubes based on the concentration of the active tile suggests a kinetic nucleation barrier. The concentrations of the incomplete and protected tiles were 200 nM. The concentrations of the activators used in method 1 were 300 nM. The concentration of the deprotector was 220 nM in the top series of figures for method 3, and 40 nM in the bottom series of figures. In all experiments, the reactants were mixed and allowed to react at room temperature (25 °C) for 2 hours prior to imaging.

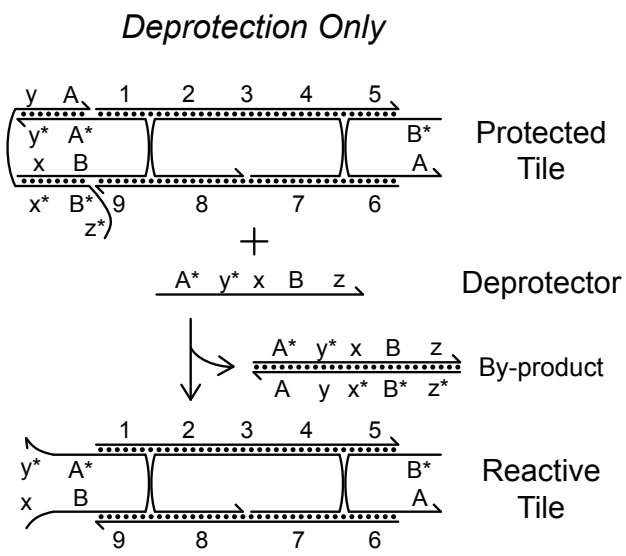

Supplementary Figure S6: Diagram of proposed method 2 for deprotecting a double-crossover tile. Unlike method 3 presented in the main text, where the deprotector strand also became an integral part of the reactive tile after displacing the two protection strands, this method does not also involve implicit activation. In the DAE-E tile architecture, the lengths of sticky end domains A^* and B^* are typically only 5 nt, and 5 base pairs dissociate with a time constant of roughly 10 ms (ref. 25 of the main text). Consequently, we appended domains x^* and y^* to the left strand of the tile to provide extra hybridization stability for the protector. The x and y domain sequences can be designed to not interact with other sticky ends, and when the tile is incorporated into a DNA nanotube assembly, these domains will be present as "hair" on the inner or outer surface of the nanotube. Like method 1, method 2 could also be applicable to DAO-E tiles, in addition to the DAE-E tiles shown here.

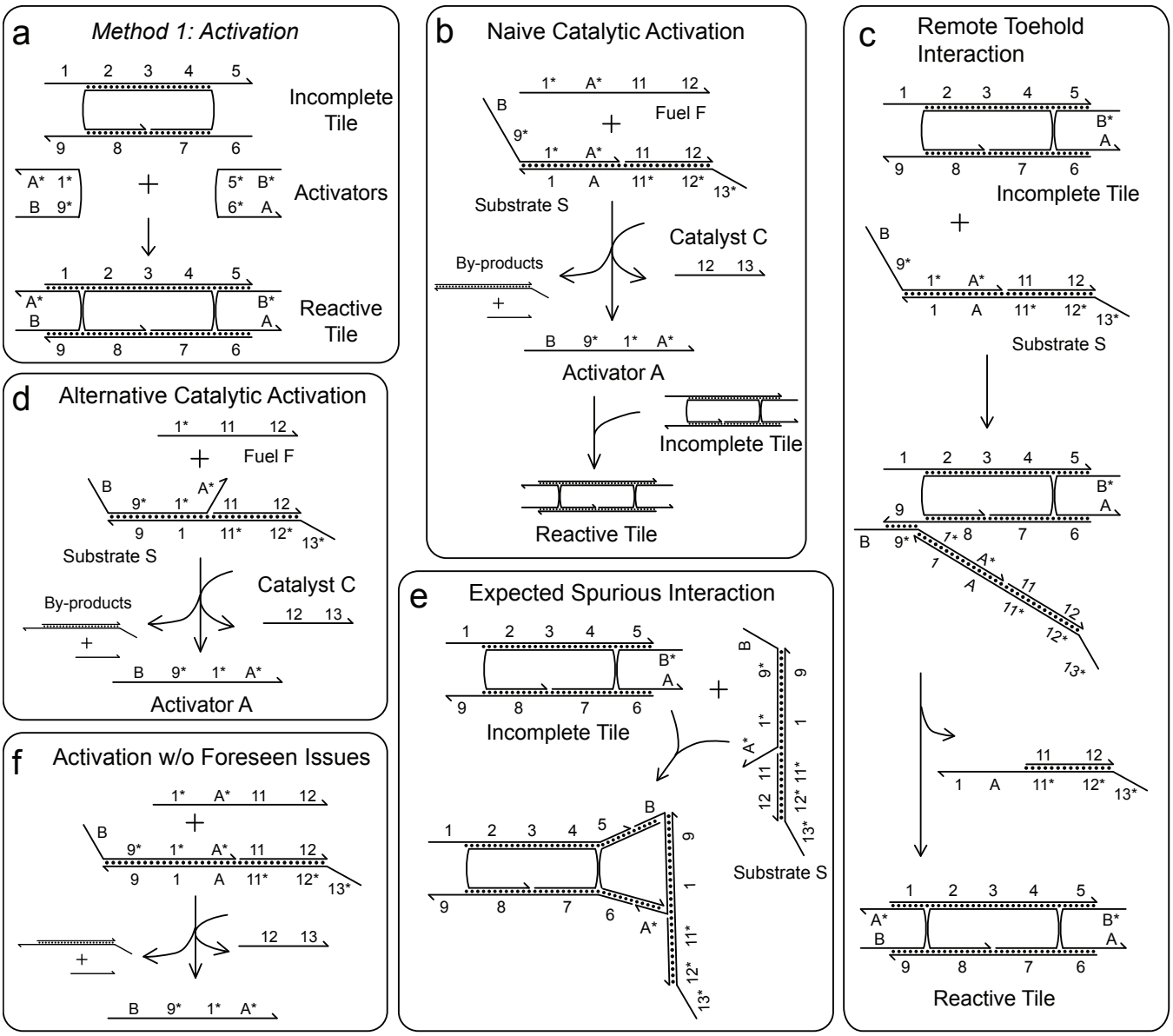

Supplementary Figure S7: Challenges for integrating method 1 with upstream catalysis. **(a)** Method 1 of triggering self-assembly using activation of incomplete tiles. **(b)** An intended catalytic reaction that produces the left activator as product. **(c)** One possible spurious interaction that can occur in the absence of the upstream catalyst. The branch migration of domain 1 bridges a crossover point, and is considered a remote toehold interaction (ref. 51). Because both the incomplete tile and the substrate are at high concentrations, this interaction is expected to be signficant; nanotubes are expected to form even in the absence of the catalyst. **(d)** An alternative implementation that produces the left activator as product. **(e)** In this alternative scheme, the substrate itself can interact with the right side of the inactivated tile.**(f)** Another alternative scheme for integrating method 1 with upstream catalysis. Although the fuel could potentially interact with the incomplete tile via the 1* domain or the A* domain, both of these domains are short (8 nt and 5 nt, respectively) so these interactions quickly dissociate, and are not significantly present at equilibrium at 25 °C. Furthermore, even with the fuel attached to the incomplete tile via the 1 and 1* interaction such that the adjacent A* domain on the fuel gives the tile another sticky end, the incomplete tile will only have 3 of the 4 sticky ends and also will not self-assemble.

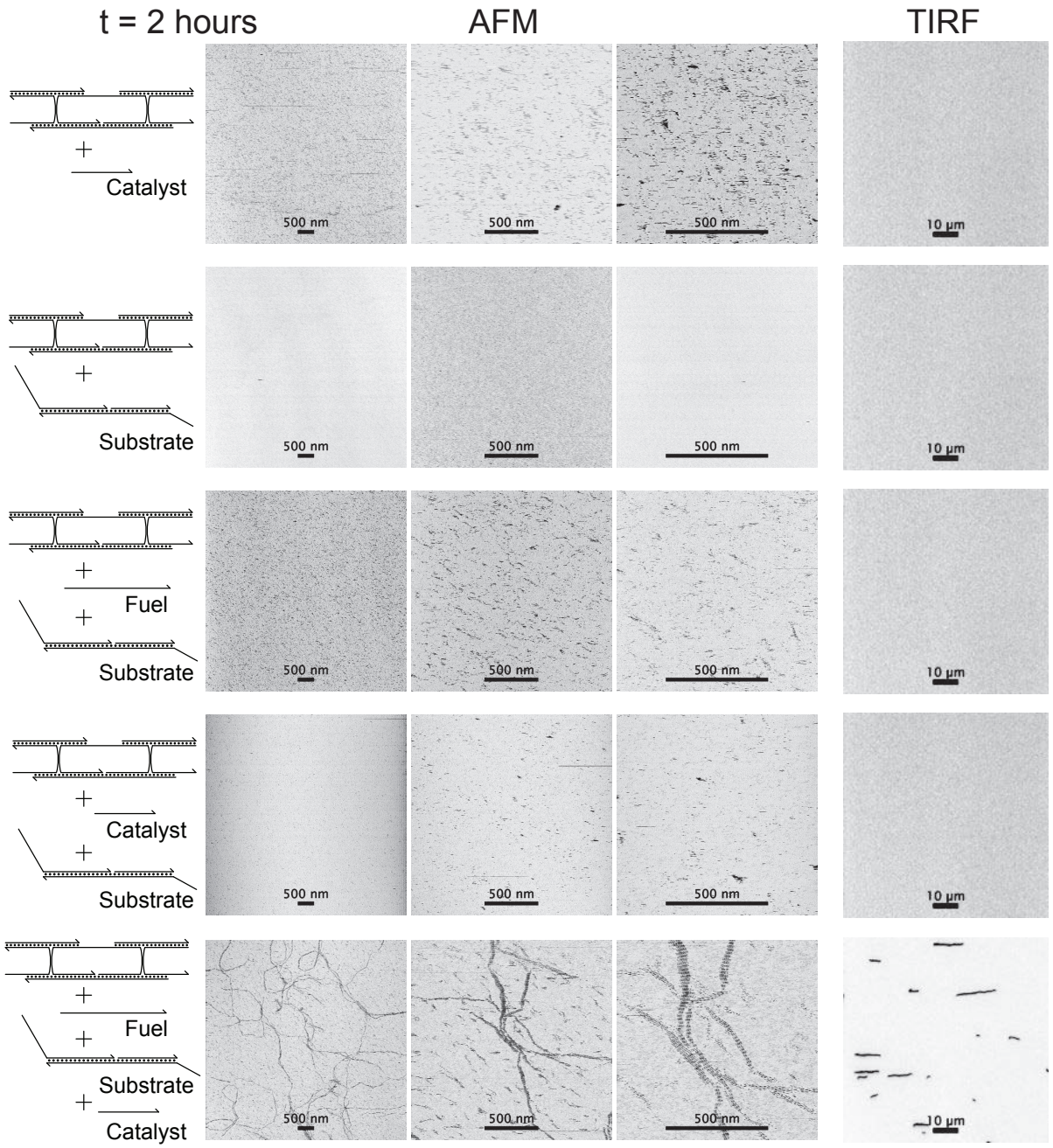

Supplementary Figure S8: Additional AFM and TIRF experiments on the integrated system (without sink). The protected tile is reacted with various components of the upstream system. DNA nanotubes are expected to form only in the bottom series of experiments. The concentrations of the protected tiles were 200 nM. The concentrations of fuel, substrate, and catalyst were 440 nM, 220 nM, and 20 nM, where applicable. In all experiments, the reactants were mixed and allowed to react for approximately 2 hours prior to imaging. No sink complex was used for the experiments shown here.

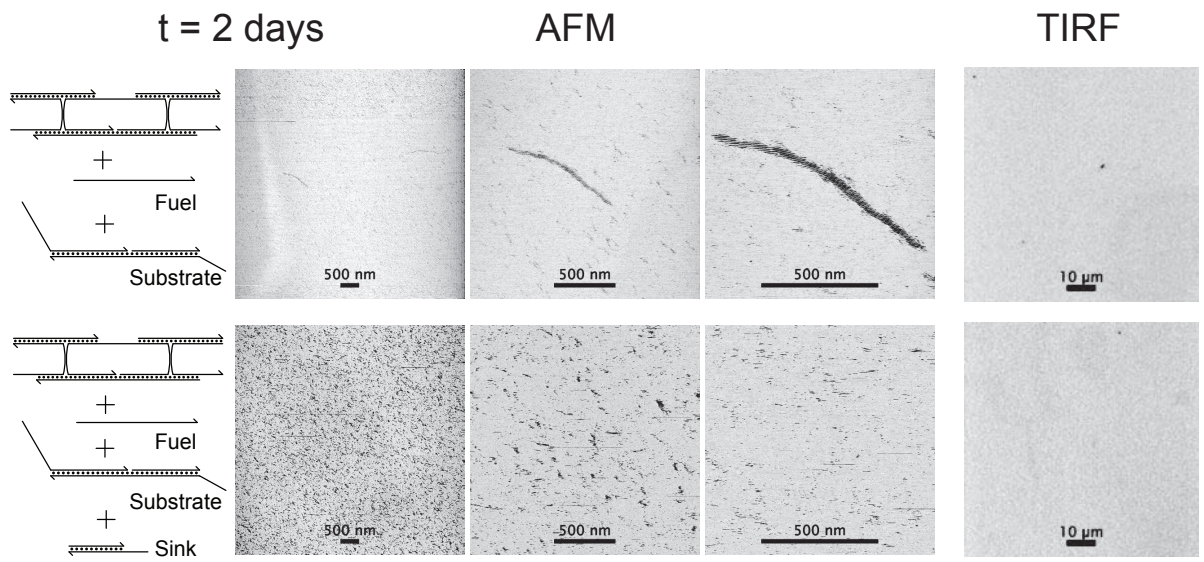

Supplementary Figure S9: Additional AFM and TIRF experiments on the integrated system (with sink). When the protected tile is reacted with fuel F and substrate S in the absence of catalyst C for 2 days, a very few nanotubes are formed; the top row of AFM images shows the only structure formation we were able to find after careful observation of many areas of the sample on mica. When a small amount of the sink complex is present, no nanotubes are observed to form even after 2 days. The concentrations of the protected tile (PT), fuel, and substrate were 200 nM, 440 nM, and 220 nM. The concentration of the sink complex was 40 nM.

Supplementary Methods

TIRF Analysis. For quantification of DNA nanotube assembly kinetics (e.g. main text Fig. 5), we assumed that the fluorescence intensity per pixel F in an image (after signals from the fiducial fluorescent beads have been subtracted) is proportional to the total amount of DNA tiles in tube form, since tile monomers are not confined to the surface and thus not excited by the laser.

To perform the normalization, we first subtracted a background fluorescence signal $F_{\text{Background}}$ from the photon counts. The background signal was calculated by averaging the photon count in the first 3 minutes of the movie for all runs other than the 1.5× deprotector reaction (green trace in Fig. 5 of the main text). The average background signal varied by less than 2% from movie to movie; consequently, we used the average of these values as the background.

We then normalized all of our background-subtracted photon counts by dividing that value by the expected photon counts after reactions reach equilibrium. The photon counts of the 1.5× deprotector experiment $F_{1.5\times D}$ (green) and the 0.2× catalyst experiment $F_{0.2\times C}$ (red) plateaued after 25 and 35 minutes, respectively, after which all photon counts were within 5% of the mean; this indicates that photobleaching was not significant at the time scale of the experiments. The average of the plateaued values of the 1.5× deprotector experiment and the 0.2× catalyst experiment were within 6% of each other, and the average of these two values were taken to be the maximum signal $F_{\max}$ (normalized to 1), used to normalize photon counts from all movies. Notably, the 1.5× deprotector trace and the 0.2× catalyst traces were each normalized to the average of the two, which is why the normalized photon counts for the green trace in Fig. 5 of the main text consistently exceeds 1 towards later time points. In summary:

$$\begin{aligned} F_{\text{norm}} &= \frac{F - F_{\text{Background}}}{F_{\max} - F_{\text{Background}}} \\ F_{\text{Background}} &= \frac{1}{N} \sum_{t=0\ \text{min}}^{3\ \text{min}} (F_{0.1\times D}(t) + F_{0.2\times D}(t) \\ &\qquad + F_{0.1\times C}(t) + F_{0.2\times C}(t)) \\ F_{\max} &= \frac{1}{N} \left(\sum_{t=25\ \text{min}}^{60\ \text{min}} F_{1.5\times D}(t) + \sum_{t=35\ \text{min}}^{60\ \text{min}} F_{0.2\times C}(t) \right) \end{aligned}$$

where N is the total number of data points summed for each expression.

Images were collected at 2 frames per minute (100 ms exposure time) and the autofocus routine was performed once per minute, which may account for the oscillatory noise in the total intensity measurements. Movies were recorded simultaneously at high, medium, and low CCD gains; to avoid supersaturated pixels, only medium gain images were analyzed. The first movie frame ($t = 0$) is the first image collected after mixing the sample, loading the sample into the capillary chamber, setting up the imaging software, and starting the autofocus routine – a process which takes less than 1 minute.

We relate the normalized fluorescence photon counts, F_{norm} to the concentrations of Monomers (i.e. activated tiles) and PT (i.e. protected tiles) according to

$$F_{\text{norm}} = \frac{[PT]_0 - [PT] - [\text{Monomer}]}{[PT]_0}$$

where $[PT]_0$ is the initial concentration of protected tile (in this case, 200 nM). Rephrased, F_{norm} is the fraction of initial protected tiles that are neither free activated tiles nor free protected tiles, i.e. they are incorporated into tubes. To be approximately correct, this formula relies on the assumption that almost all DNA nanotubes are localized on the surface where their fluorescence can be measured. In point of fact, experience suggests that DNA nanotubes deposit onto the surface and remain there (due to the effects of the crowding agent) only after they have grown large enough (perhaps on the order of 1 μm); however, we estimate that this is an insignificant inaccuracy. Another caveat is that because of bundling of the

DNA nanotubes (again due to the effects of the crowding agent) we cannot directly measure the length distribution of tubes, and we must assume that the fluorescence of bundles is linear in the total amount of incorporated monomers in all the tubes of the bundle.

Fitting kinetic model to catalysis results. The four catalysis rate constants shown in Table 2 (k_{bi1}, k_{bi2}, k_{uni}, and k_{leak}) were fitted to the traces shown in Supplementary Fig. S3de. Kinetic model fitting was done using MATLAB's "fminunc" function, using the "ode23s" function to simulate the various ordinary differential equations describing the trajectory of the concentrations. For ode23s, the relative tolerance was set at 10^{-4}. The error function is calculated as follows:

$$\begin{aligned}\text{Error} \;=\; & \sum_{\text{traces}} \left(\frac{1}{N} \sum_{i=1}^{N} \left(\frac{\text{Data}(i) - \text{Model}(i)}{[S_{\text{init}}]} \right)^2 \right) \\ & + \frac{99}{N} \sum_{i=1}^{10} \left(\frac{\text{Data}_{\text{Fig. S5e-red}}(i) - \text{Model}_{\text{Fig. S5e-red}}(i)}{[S]_{\text{init}}} \right)^2\end{aligned}$$

where N is the number of data points for each trace ($N = 180$ for the four traces in Supplementary Fig. S3d, and $N = 410$ for the two traces in Supplementary Fig. S3e) and $[S]_{\text{init}}$ is the initial concentration of S (the limiting reagent). The first term denotes the normalized square error for each trace, and the second term denotes an adjustment term to overweight the initial data ($t < 25$ min) of the $[S] = 200$ nM, $[C] = 1$ nM trace that is most relevant to time scales of the tube assembly experiments.

The adjustment term exists because the catalysis model tends to predict both a faster initial rise and a sharper slowdown at later timepoints than observed experimentally. The best-fit parameters for the error function without the adjustment tends to a significantly smaller k_{uni} that is not consistent with the integrated system results as observed by TIRF. The adjustment parameters (99-fold overweight for the first 10 data points) were chosen *ad hoc* and were not optimized for improving the fit for the integrated system.

Fitting kinetic model to TIRF results. The rate constants k_{deprot}, k_{sink}, k_{nuc}, and the stoichiometry n were fitted to five of the traces shown in Fig. 5 of the main text (all but the cyan $0\times$ catalyst trace). Kinetic model fitting was done using MATLAB's "fmincon" function, with k_{deprot} and k_{sink} being constrained between 10^5 and 10^7 M^{-1} s^{-1}, consistent with expected rate constants for such strand displacement reactions (ref. 25). Again, the "ode23s" function was used to simulate the various ordinary differential equations describing the trajectory of the concentrations. The error function is calculated as a normalized sum of squares:

$$\text{Error} \;=\; \sum_{\text{traces}} \left(\frac{1}{N} \sum_{i=1}^{N} \left(\frac{\text{Data}(i) - \text{Model}(i)}{[PT]_{\text{init}}} \right)^2 \right)$$

where N is the number of data points modeled for each trace ($N = 90$ for $0.1\times$ catalyst trace, $N = 120$ for all other traces) and $[PT]_{\text{init}}$ is the intial concentration of protected tile PT. Note that classical mass action rates are assumed for all reaction equations, and that the flux for equation (8) is taken to be $\frac{d}{dt}[\text{Monomer}] = -n \cdot k_{nuc} \cdot [\text{Monomer}]^n$, even though n may be a non-integer real number.

Supplementary Notes

Supplementary Note 1: Application of method 1 as AND logic gate. One interesting feature of this design is that the incomplete tile lacking both sticky end-bearing strands functions as a Boolean AND gate, because both activators must be present to induce DNA nanotube formation. This opens up the potential for designing more complicated control circuits that result in the formation of complex DNA self-assembled structures. On the other hand, tile activation using only a single trigger species may be faster kinetically and simpler to integrate with other systems; this was experimentally achieved by having one of the activators pre-annealed into the incomplete tile.

Supplementary Note 2: Method 3 threading timescale. At 1 μM DNA concentrations, hybridization of complementary DNA strands occurs on the time scale of seconds (ref. 25). Three-way branch migration processes occur at the 10 μs time scale; thus threading must slow down branch migration by over 5 order of magnitude to significantly affect kinetics at sub-micromolar concentrations, which we consider to be unlikely.

Supplementary Note 3: Reversibility of the catalytic reaction pathway. Unlike in the standard catalyst system described in (ref. 27), here we truncated 7 bases off the fuel, so that the net reaction ($F + S \rightarrow D + B1 + B2$) has a free energy change of +1 entropy contribution and -7 base pair contributions. Thermodynamically, this is almost balanced at the concentrations we work with: at 200 nM, the entropy component is $RT \cdot \ln(200\text{ nM}/1\text{ M}) = -9.14$ kcal/mol, while the base pair component at 25 °C is approximately -10.83 kcal/mol according to nearest neighbor models calculated as in (ref. 25). Consequently, at equilibrium and in isolation, we will have a significant concentration of fuel F and substrate S in addition to deprotector D and by-products $B1$ and $B2$.

However, the catalyst system is not in isolation. For the fluorescence experiments, we have a reporter complex that acts as a sink, and for the integrated experiments, we have the precursor tiles that act as a sink. Consequently, the reverse reaction is not significant, because in our experiments there is always more reporter or precursor tile than by-product $B2$, and thus free deprotector is most likely to first react with a sink species.

Kinetically, when both catalyst C and deprotector D are bound to by-product $B2$ in the first step of the reverse reaction pathway, there is an approximately 1 in 400 equilibrium probability that both branch migrations have proceeded to where the fuel F is bound by only the internal toehold. The expected time for spontaneous dissociation of the internal toehold (5 base pairs involving 6 nearest-neighbor stacking interactions) can be estimated (c.f. Fig. 7A of ref. 25) as roughly 1 s, so the expected time for the reverse reaction to occur (and the fuel to dissociate) will be roughly 400 s. Based on this estimate, we believe that the reaction should reach equilibrium in a few minutes.

Supplementary Note 4: TIRF signal interpretation. For the purposes of this model we assume that all DNA nanotubes that successfully nucleate within the field of the TIRF microscope are immediately but lightly adsorbed to the surface such that they can continue to grow their while being clearly imaged. In Movies S1-S4, we see that this assumption may be inaccurate — only nanotubes of 1 μm or longer appear to be deposited on the surface, and DNA nanotubes "join" both laterally (ref. 52) and longitudinally (ref. 40). Modeling the DNA nanotube deposition and joining processes may further quantitatively improve the agreement between model and experiments, but would also introduce significant extra complexity. We did not pursue these, as our current simplified model does seem to effectively describe the features of the integrated system (Fig. 5 of the main text).